LETTERS

Anticipatory haemodynamic signals in sensory cortex not predicted by local neuronal activity

Yevgeniy B. Sirotin[1] & Aniruddha Das[1,2,3,4,5,6]

Haemodynamic signals underlying functional brain imaging (for example, functional magnetic resonance imaging (fMRI)) are assumed to reflect metabolic demand generated by local neuronal activity, with equal increases in haemodynamic signal implying equal increases in the underlying neuronal activity[1–6]. Few studies have compared neuronal and haemodynamic signals in alert animals[7,8] to test for this assumed correspondence. Here we present evidence that brings this assumption into question. Using a dual-wavelength optical imaging technique[9] that independently measures cerebral blood volume and oxygenation, continuously, in alert behaving monkeys, we find two distinct components to the haemodynamic signal in the alert animals' primary visual cortex (V1). One component is reliably predictable from neuronal responses generated by visual input. The other component—of almost comparable strength—is a hitherto unknown signal that entrains to task structure independently of visual input or of standard neural predictors of haemodynamics. This latter component shows predictive timing, with increases of cerebral blood volume in anticipation of trial onsets even in darkness. This trial-locked haemodynamic signal could be due to an accompanying V1 arterial pumping mechanism, closely matched in time, with peaks of arterial dilation entrained to predicted trial onsets. These findings (tested in two animals) challenge the current understanding of the link between brain haemodynamics and local neuronal activity. They also suggest the existence of a novel preparatory mechanism in the brain that brings additional arterial blood to cortex in anticipation of expected tasks.

We have developed a dual-wavelength optical imaging technique to (in effect) image cortical blood volume and oxygenation simultaneously in alert behaving macaques. This technique involves switching rapidly between two wavelengths: 530 nm (green, equally absorbed in oxygenated and deoxygenated haemoglobin, thus measuring total haemoglobin concentration (HbT) or 'blood volume') and 605 nm (red, absorbed about fivefold more strongly in deoxygenated than oxygenated haemoglobin, thus measuring 'oxygenation'[10]

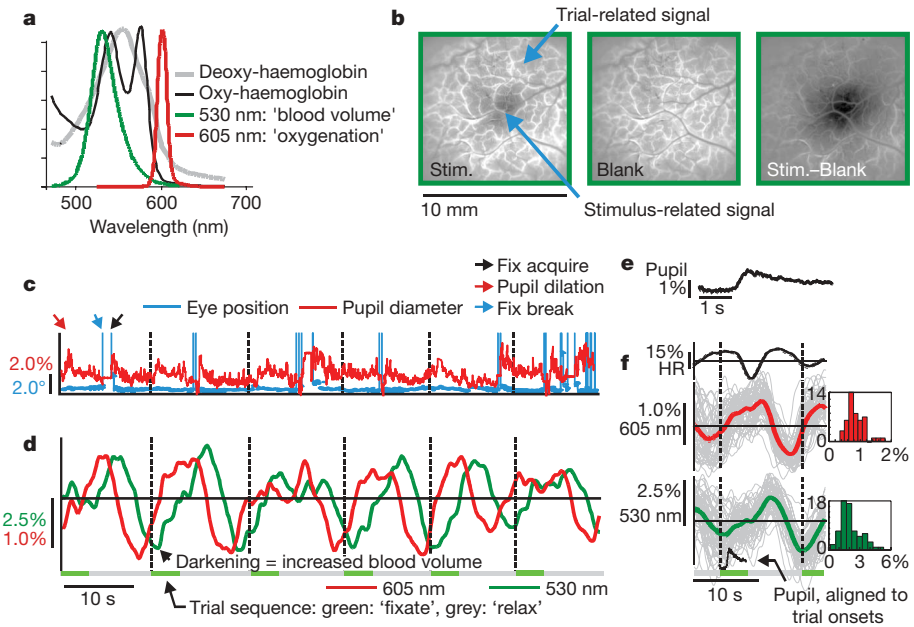

Figure 1 | Periodic fixation tasks evoke stimulus-independent, trial-linked signals even in the dark. **a**, Normalized emission spectra of the two illumination sources (light-emitting diodes), superimposed on *in vitro* absorbance spectra for deoxy- and oxyhaemoglobin[10] (units: $10^4\,cm^{-1}\,M^{-1}$). **b**, Stim.: V1 'blood volume' response to small, brief, visual stimulus presented during periodic fixation trials. 'Blank': signal in trial with no visual stimulus. 'Stim.-Blank': stimulus-specific response. **c**, Eye position and pupil diameter (percentage of mean), consecutive trials. (Vertical dashed lines: trial onsets. Note pupil dilation, fix break, fix acquire, shown for first trial.) Scales are colour-coded. **d**, Cortical signals, colour-coded by imaging wavelength. **e**, **f**, Trial-triggered averages (grey lines, individual trials; thick lines, mean ± s.e.m., $n = 51$: at 605 nm, mean peak-to-peak amplitude = 1.19% ± 0.08; at 530 nm, 3.47% ± 0.21). Population histograms: at 605 nm, mean = 0.86%, s.d. = 0.29, $N = 47$ experiments; at 530 nm, mean = 2.17%, s.d. = 0.97, $N = 66$.

[1]Department of Neuroscience, [2]Department of Psychiatry, [3]W. M. Keck Center on Brain Plasticity and Cognition, [4]Mahoney Center for Brain and Behavior, [5]Department of Biomedical Engineering, Columbia University, New York, New York 10027, USA. [6]New York State Psychiatric Institute, 1051 Riverside Drive, Unit 87, New York, New York 10032, USA.

(Fig. 1a and Supplementary Methods)). While imaging V1 in animals performing periodic visual tasks, we observed a hitherto unknown stimulus-independent haemodynamic signal that appeared to entrain to trial timing (Fig. 1b).

To study this trial-related signal in isolation, we developed a task that minimized visual input while preserving trial timing. In an otherwise completely dark room, the animal was required to fix its gaze periodically on a tiny fixation point for juice reward (point size about 1–2 arcmin, that is, about 1–2 cone diameters). The fixation point stayed on continuously, switching between two equiluminant colours to cue the animal to 'fixate' or 'relax'. It was akin to seeing nothing apart from one single twinkling star in an otherwise black night sky. Our two rhesus macaque monkeys ('V' and 'S') learned the task correctly, as evidenced by their fixation patterns (Fig. 1c). Both monkeys performed long sequences of correct trials, consistently holding fixation during 'fixate' periods and taking fixation breaks, if any, only during 'relax' periods.

On imaging V1 while the animals performed this task, we observed robust haemodynamic signals at the trial frequency, even though the animals were in virtually total darkness and foveal V1, the only region receiving visual input from the fixation point, lay outside our imaging area. These periodic fluctuations were seen in both the 'blood volume' (530 nm) and 'oxygenation' signals (605 nm; Fig. 1d, f). They were accompanied by periodic changes in heart rate[11] and systematic pupil dilation[12] on trial onset, suggesting a rhythmic state of alertness synchronized to each trial (Fig. 1c–f).

We wanted to determine the relation between these trial-linked haemodynamic signals and V1 neuronal activity. A crucial assumption in most brain imaging studies is that haemodynamic signals are caused by local neuronal responses through a uniform underlying mechanism[1–6] (but see refs 13, 14). In particular, brain images are routinely used to infer changes in local neuronal activity by fitting the imaging signal with some standard causal haemodynamic kernel. To reveal neuronal mechanisms underlying V1 haemodynamics, we obtained both trial-related and visually evoked optical imaging signals concurrently with electrode recordings across V1 (Supplementary Fig. 1 and Supplementary Table 1). At each site, in alternating blocks (20–40 trials each) while the animal performed the same fixation task, we presented either vigorous visual stimuli or no stimuli at all. For each data set we then used an optimization routine to calculate the causal kernel that 'best' fitted haemodynamics to concurrent neuronal signals (Supplementary Fig. 2), and tested whether this 'best' kernel could reliably predict haemodynamics.

To get measures of neuronal activity for this analysis, we separated the electrode recordings into multi-unit spiking (MUA) and local field potential (LFP) (Supplementary Fig. 1 and Supplementary Methods). As expected, visual stimulation evoked vigorous responses in both MUA and LFP (Fig. 2a). The stimulus-evoked LFP responses could

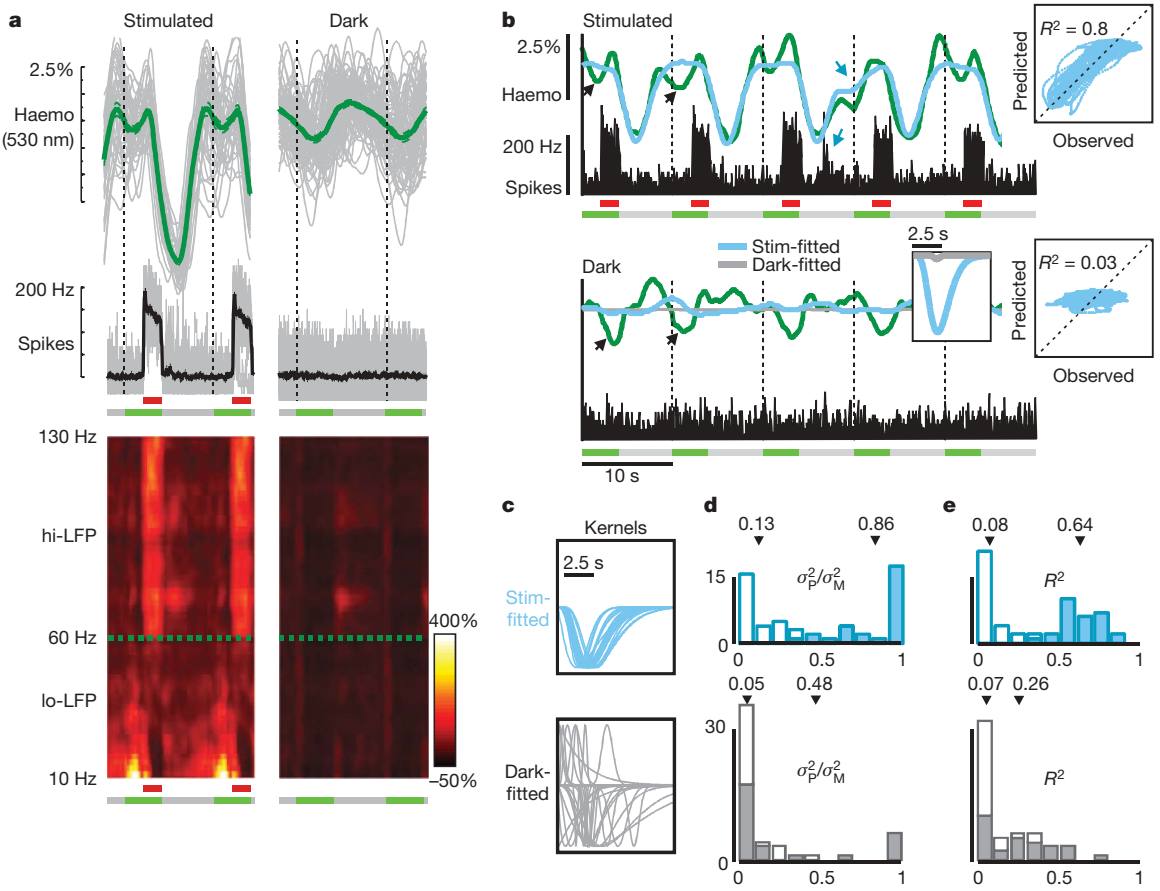

Figure 2 | Local neuronal activity predicts visually driven, but not trial-related, haemodynamics. **a**, Trial-triggered mean haemodynamic ('blood volume') and electrophysiological signals comparing stimulus-driven and dark-room responses, representative experiment. LFP power spectrum (bottom) normalized to pre-stimulus dark power (2-Hz resolution). **b**, Comparing measured haemodynamics (green) with optimal predictions from concurrent spiking, same experiment. Blue, grey: using kernels (inset) obtained by fitting stimulated or dark-room signals respectively. (The same colour code is used throughout. Dark-room kernel and prediction almost indistinguishable from a flat line; prediction shown for dark only, to avoid clutter.) Black arrows: trial-related activity not predicted in either the stimulated or dark-room trials. Blue arrows: random bursts of neuronal activity generate matching deflections in the predicted and observed trace. Right: scatter-plots and R^2 values of observed versus predicted haemodynamics using stimulus-based predictors. **c**, Optimal kernels across days (amplitude normalized for comparison; $N = 28$ recording sites). **d**, **e**, Descriptive statistics of spike-based fits. Top: stimulus-based prediction; bottom: dark-room based. **d**, Ratio of variance between predicted and measured signals (σ_P^2/σ_M^2). **e**, R^2 statistic: open versus closed bars represent dark-room versus stimulus-driven sessions, respectively. Arrows mark population means.

be empirically separated into two distinct frequency bands (Fig. 2a, bottom). The high-frequency band (hi-LFP: 66–130 Hz, avoiding 60 Hz), like MUA, showed crisp, visually evoked responses. The low-frequency band (lo-LFP: 10–56 Hz), also showed a robust signal but with no apparent correlation with visual stimulation. Our empirically defined LFP bands match categories defined through previous work. The hi-LFP matches a frequency band ('high gamma') that is shown to correlate well with stimulus-evoked spiking and haemodynamics[2,15,16]. The lo-LFP—often separated into finer frequency bands[15,16]—is believed to have a very different relationship with other brain signals[15,16]. We therefore decided to test the three neuronal signal types, MUA, hi-LFP and lo-LFP, independently for their ability to predict concurrently recorded haemodynamics reliably. These tests were conducted separately for 'blood volume' and 'oxygenation' signals.

Visually driven MUA and hi-LFP predicted the simultaneously recorded haemodynamic signals very well both in amplitude and time course (Fig. 2b–e and Supplementary Fig. 3b–e). Further, the optimal kernels obtained by fitting these signals were consistent in shape across all recording sites (Fig. 2c and Supplementary Fig. 3c, top); kernels from any given experiment predicted visually evoked responses in all other experiments with almost equal accuracy, attesting to their remarkable reliability (Supplementary Fig. 4). In sharp contrast, the same kernels, when convolved with dark-room MUA or hi-LFP, were uniformly poor at predicting trial-related haemodynamics, in both amplitude and temporal correlation (Fig. 2b–e and Supplementary Fig. 3b–e). The latter finding ($R^2 \sim 0.08$, MUA; 0.06, hi-LFP) specifically implies that there is no consistent temporal relation between predicted and measured haemodynamics, independent of amplitude. This poor predictability was particularly striking because the trial-related haemodynamic signal amplitudes were almost comparable to those of responses to vigorous visual stimulation (37% at 'blood volume', 530 nm; 57% at 'oxygenation', 605 nm (Supplementary Fig. 5)). To check whether trial-related haemodynamics could still be predicted reliably by concurrent neuronal recordings but through kernels of a different shape, we fitted dark-room MUA and hi-LFP to dark-room haemodynamics. These 'best' dark-room kernels were highly variable among recording sites and, again, consistently failed to predict trial-related haemodynamics (Fig. 2c–e and Supplementary Fig. 3c–e, bottom). The same overall pattern of results was seen for both 'blood volume' and 'oxygenation' signals (Supplementary Fig. 6).

These results provide compelling evidence that visually evoked haemodynamic signals are very well predicted by established measures of local neuronal activity (MUA, hi-LFP) through a causal kernel that is uniform across experiments. Such a model fails profoundly, however, to predict the trial-related signals. Therefore any neuronal mechanisms underlying trial-related haemodynamics appear to be distinct from those typically assumed to underlie neurovascular coupling.

Unlike MUA or hi-LFP, lo-LFP—whether treated as a whole or separated into finer frequency bands—failed to show any consistent relationship with haemodynamics. These signals gave highly variable 'optimal kernels' when fitted with concurrent haemodynamics either under visual driving or in the dark, with uniformly poor predictions of haemodynamics (Supplementary Figs 7 and 13).

Next, we characterized the novel trial-related haemodynamic signal in terms of its temporal relation to trial timing. To determine whether our observed signals are linked specifically with trial timing and not a result of some unrelated intrinsic oscillatory process[17], we examined how the signals adapted to different trial periods. Our results provided compelling evidence that the signals are linked predictively to trial onsets. This was seen both in the signal shapes at each trial period and their anticipatory timing on switching trial period.

We found that the trial-related signals stretched elastically to match each tested trial period (Fig. 3 and Supplementary Fig. 8a; tested 6-s to 30-s trial periods). In particular, the shape of the 'blood volume' signal

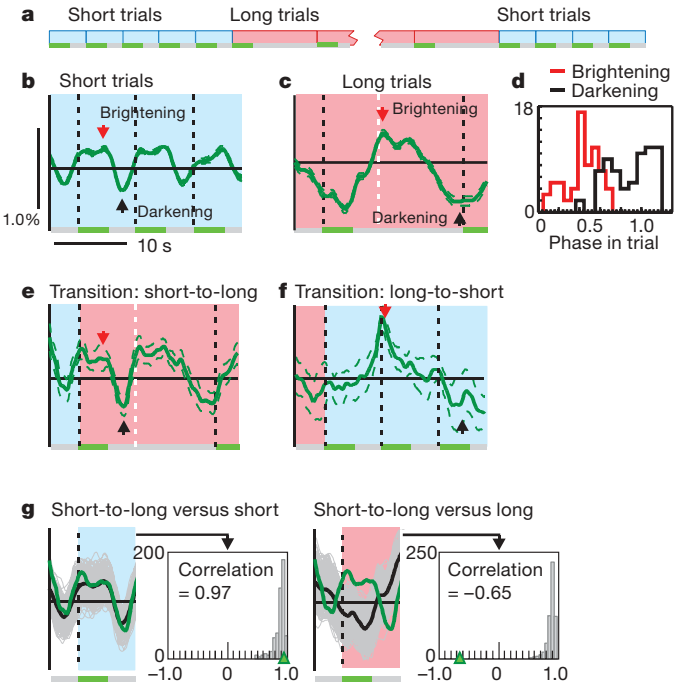

Figure 3 | Trial-related haemodynamic signals entrain to anticipated trial onsets, stretching to conform to the trial period. **a**, Dark-room fixation trials, each with the same 4-s 'fixate' epochs but in blocks of different trial periods, short (8 s, blue) and long (20 s; pink) (same colour scheme in other panels and Fig. 4). **b**, **c**, 'Blood volume' signal, short and long trials respectively. Averages triggered on trial onsets, ± s.e.m. (**b**: $N = 220$ trials; **c**: $N = 179$). Arrowheads: peak brightening (red), darkening (black). Dotted white line in **c** shows where short-trial onset would have occurred. **d**, Population histograms of peak brightening and darkening in units of trial phase (0, trial start; 1, trial end, start of next trial; brightening, mean = 0.43, s.d. = 0.16; darkening, mean = 0.89, sd = 0.21; $N = 66$; trial periods ranged from 6 to 30 s). **e**, **f**, Signal at transitions between trial periods: short-to-long (**e**, $N = 16$ trials, mean ± s.e.m.), and long-to-short (**f**, $N = 10$); arrowheads are aligned, in each case, to the panel above for comparison of signal features. Dotted white line as in **c**. **g**, Left: short-to-long transition trial (green) is statistically indistinguishable from other short trials over one short-trial period (blue background). (Bootstrap analysis. Green: mean transition trial; grey: means of 500 random $N = 16$-trial subsets of the short trials to match statistics of transition trial; black: grand mean of all short trials, same as **b**; inset histogram: correlation of random subsets with grand mean; arrowhead: correlation of transition trial with grand mean = 0.97.) Right: short-to-long transition response is distinct from random $N = 16$-trial subsets of long trials. Same conventions as on the left, with the correlation coefficients being calculated, again, over the duration of one short period (pink background).

always stretched so as to start darkening (increasing haemoglobin) during the 'relax' period—before the onset of the next trial—reaching a peak darkening close to the onset of the next 'fixate' period (Figs 1 and 3a–d). This elastic pattern of trial-locked haemodynamics—in which signals begin changing before trial onsets—cannot be explained by mechanisms that involve a causal kernel triggered on trial start. This can be demonstrated by comparison with responses to (brief, intense) visual stimulation of the same duration as the 'fixate' period, where the stereotyped response shape, with abrupt onset and fixed width after stimulus presentation, is independent of trial period (Supplementary Fig. 8b; quantitative model, Supplementary Fig. 8c). The trial-related signal is thus unlikely to be due to neuronal signals active only during the cued 'fixate' period (for example, the presumed time course of 'attention'[18]).

On switching trial timing unexpectedly after the monkey had established a rhythm of 10–20 correct trials at a given period, haemodynamic signals continued to oscillate at the earlier period for a couple of trials before entraining to the new one (Fig. 3e, f). This

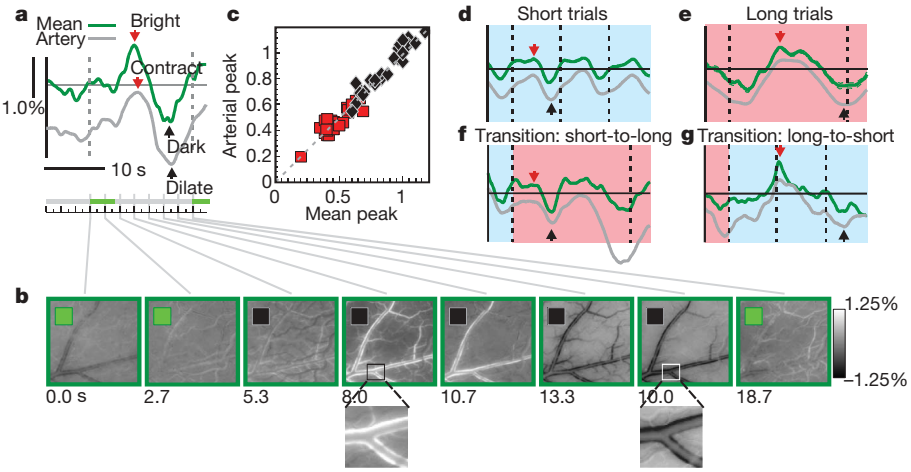

Figure 4 | Mean 'blood volume' signal is closely matched, temporally, by V1 arterial contraction–dilation cycle. **a**, Mean trial-triggered signals and **b** individual frames showing fractional signal change relative to trial-mean image. Inset square: green, 'fixate'; black, 'relax'. Magnified sections show arterial contraction (white walls) and dilation (black walls). Grey trace in **a**: arterial signal relative to 'parenchyma baseline' (Supplementary Fig. 11, method for calculating arterial signal; arterial trace shifted vertically from overall mean for visibility). **c**, Timing of peak arterial contraction (dilation), as phase within trial, matches peak brightening (darkening) of mean signal: red square (black diamond) respectively. **d–g**, Arterial signal (grey) closely matches mean signal (green) for different trial periods (**d**, **e**) and at transitions between periods (**f**, **g**); same experiment, conventions as in Fig 3b, c, f, g (traces shifted vertically for visibility). Note close matches between corresponding peaks and troughs (arrows), indicated as in Fig. 3.

occurred even though the animal itself picked up the new trial pace immediately, holding and breaking fixation at the new rhythm right after the switch (that is, clearly having noticed the new pace of fixation cues). Thus, on switching from short to long trials the measured signals showed a peak darkening at the short-trial spacing even though the animal was fixating correctly at the longer period (Fig. 3e). Similarly, on switching from long to short trials the cortical signal continued at its previous slower pace for one long period, overriding the first few short trials (Fig. 3f). The response shape observed on transition trials closely resembled pre-transition responses for the duration of the pre-transition trial period, while being very poorly matched to the post-transition trial shape, suggesting that the underlying neuronal mechanism continued to 'anticipate' the pre-transition trial timing (Fig. 3g and Supplementary Fig. 9). Further, the trial-related signal timing was correlated specifically with trial onsets and not with reward[19]: the peak darkening position remained unaffected on delaying the reward associated with each trial (Supplementary Fig. 8d).

Finally, images of the cortical surface suggested that the trial-related signals involve the local vasculature rather than being a systemic trial-locked autonomic (for example, cardiac) response[20]. These images revealed a dramatic contraction–dilation cycle in V1 arteries, evidenced by a prominent brightening, followed by darkening of the arterial walls relative to the 'parenchyma' baseline (Fig. 4a, b and Supplementary Fig. 10; Supplementary Fig. 11 indicates how arteries, veins and 'parenchyma' are distinguished and how the arterial signal is measured). This arterial signal had a timing that closely matched the overall timing of the mean 'blood volume', with peaks of arterial contraction and dilation coinciding with peaks of brightening (decreased haemoglobin) and darkening (increased haemoglobin), respectively (Fig. 4a, c–g). The arterial cycle stretched elastically to fit trial periods, matching the shape of the mean signal (Fig. 4d, e). Further, on switching trial periods, the arterial cycle showed an anticipatory dilation that was well synchronized with the anticipatory increase in 'blood volume' seen in the mean signal (Fig. 4f, g). This local arterial cycle may thus be the specific mechanism generating trial-related increases in V1 'blood volume' in anticipation of visual tasks. Further, the arterial cycle is seen in V1 only for visual tasks and is likely not a passive consequence of trial-locked changes in heart rate or blood pressure[20]. We found no V1 arterial pumping or trial-related changes in V1 'blood volume' in a periodic auditory control task, despite the presence of periodic changes in heart rate and pupil dilation very similar to those seen in our visual task (Supplementary Fig. 12).

Our findings have two major implications: one for the interpretation of brain imaging[21], the other advancing our knowledge of brain mechanisms underlying anticipation. First, the interpretation of fMRI[22], for example, through general linear modelling[23], typically makes the crucial assumption of a uniform linear predictive relationship between neuronal and haemodynamic signals. We show that this model is valid for visually evoked signals, but that it fails profoundly to predict another class of signals, of almost comparable magnitude and behaviourally linked structure. These results raise the further possibility that there may be other, hitherto uncovered exceptions[13,14] to the assumption that haemodynamic signals uniformly imply equivalent underlying neuronal activity. Second, the predictive timing and arterial contraction–dilation cycle that we observe in the trial-related haemodynamic signal suggests that it could reflect a novel anticipatory brain mechanism. This mechanism could play the role of preparing cortex for anticipated tasks by bringing additional arterial blood in time for task onsets. The question of the mechanism driving this signal (for example, distal neuromodulatory control of cerebral arteries?) and its functional consequences remains a challenge for future investigations.

METHODS SUMMARY

Results were obtained using continuous, dual-wavelength intrinsic-signal optical imaging and electrode recording in two monkeys engaged in either visual fixation tasks or auditory control tasks. Standard alert-monkey optical imaging techniques[24] were used to record the intrinsic cortical signal, continuously, through a clear silicone artificial dura and glass-fronted recording chamber implanted over the V1 of the animals. The primary innovation here consisted of our using two imaging wavelengths. Two arrays of fast, high-intensity light-emitting diodes at the two wavelengths (530 nm, 605 nm) were switched on and off alternately in synchrony with the camera, thus illuminating the brain surface alternately with each wavelength on successive camera frames (15 frames per second). The illumination alternated much faster than typical haemodynamic signal timescales giving, in effect, simultaneous optical imaging at both wavelengths at 7.5 frames per second. Increased absorption (darkening) at 530 nm indicated an increase in total haemoglobin ('blood volume'). Increased absorption at 605 nm primarily indicated an increase in deoxyhaemoglobin, from a combination of increased deoxygenation and blood volume.

For the dark-room fixation task, in a completely dark room, with a mask covering even the stimulus presentation monitor, the animal was cued to fixate or relax by the colour of a fixation point visible through a pinhole in the mask (size 1–2 arcmin), typically switching between equiluminant green ('fixate') and red ('relax'). We dark-adapted alongside the animal to confirm that nothing else

was visible. Control experiments confirmed that the trial-related signal was independent of the brightness (range: 10×), colour and size (range: 25× in area) of the fixation point.

All experimental procedures were performed in accordance with the National Institutes of Health Guide for the Care and Use of Laboratory Animals and were approved by the Institutional Animal Care and Use Committees of Columbia University and the New York State Psychiatric Institute.

Full Methods and any associated references are available in the online version of the paper at www.nature.com/nature.

Received 29 May; accepted 24 November 2008.

1. Logothetis, N. K. & Wandell, B. A. Interpreting the BOLD signal. *Annu. Rev. Physiol.* **66,** 735–769 (2004).
2. Logothetis, N. K., Pauls, J., Augath, M., Trinath, T. & Oeltermann, A. Neurophysiological investigation of the basis of the fMRI signal. *Nature* **412,** 150–157 (2001).
3. Vanzetta, I. & Grinvald, A. Increased cortical oxidative metabolism due to sensory stimulation: implications for functional brain imaging. *Science* **286,** 1555–1558 (1999).
4. Ugurbil, K., Toth, L. J. & Kim, D.-S. How accurate is magnetic resonance imaging of brain function. *Trends Neurosci.* **26,** 108–114 (2003).
5. Shulman, R. G., Rothman, D. L., Behar, K. L. & Hyder, F. Energetic basis for brain activity: implications for neuroimaging. *Trends Neurosci.* **27,** 489–495 (2004).
6. Heeger, D. J., Huk, A. C., Geisler, W. S. & Albrecht, D. G. Spikes versus BOLD: what does neuroimaging tell us about neuronal activity? *Nature Neurosci.* **3,** 631–633 (2000).
7. Berwick, J. *et al.* Hemodynamic response in the unanesthetized rat: intrinsic optical imaging and spectroscopy of the barrel cortex. *J. Cereb. Blood Flow Metab.* **22,** 670–679 (2002).
8. Goense, J. B. M. & Logothetis, N. K. Neurophysiology of the BOLD fMRI signal in awake monkeys. *Curr. Biol.* **18,** 631–640 (2008).
9. Hillman, E. M. C. Optical brain imaging in vivo: techniques and applications from animal to man. *J. Biomed. Opt.* **12,** 051402–1–051402-28 (2007).
10. Prahl, S. Tabulated molar extinction coefficient for hemoglobin in water. <http://omlc.ogi.edu/spectra/hemoglobin/summary.html> (2007).
11. van der Molen, M. W., Boomsma, D. I., Jennings, J. R. & Nieuwboer, R. T. Does the heart know what the eye sees? A cardiac/pupillometric analysis of motor preparation and response execution. *Psychophysiology* **26,** 70–80 (1989).
12. Beatty, J. Task-evoked pupillary responses, processing load and the structure of processing resources. *Psychol. Bull.* **91,** 276–292 (1982).
13. Nir, Y. *et al.* Coupling between neuronal firing rate, gamma LFP, and BOLD fMRI is related to interneuronal correlations. *Curr. Biol.* **17,** 1275–1285 (2007).
14. Maier, A. *et al.* Divergence of fMRI and neural signals in V1 during perceptual suppression in the awake monkey. *Nature Neurosci.* **11,** 1193–1200 (2008).
15. Niessing, J. *et al.* Hemodynamic signals correlate tightly with synchronized gamma oscillations. *Science* **309,** 948–951 (2005).
16. Belitski, A. *et al.* Low-frequency local field potentials and spikes in primary visual cortex convey independent visual information. *J. Neurosci.* **28,** 5696–5709 (2008).
17. Mayhew, J. E. W. *et al.* Cerebral vasomotion: a 0.1-Hz oscillation in reflected light imaging of neural activity. *Neuroimage* **4,** 183–193 (1996).
18. Ress, D., Backus, B. T. & Heeger, D. J. Activity in primary visual cortex predicts performance in a visual detection task. *Nature Neurosci.* **3,** 940–945 (2000).
19. Shuler, M. G. & Bear, M. F. Reward timing in the primary visual cortex. *Science* **311,** 1606–1609 (2006).
20. Franceschini, M. A., Joseph, D. K., Huppert, T. J., Diamond, S. G. & Boas, D. A. Diffuse optical imaging of the whole head. *J. Biomed. Opt.* **11,** 054007 (2006).
21. Attwell, D. & Iadecola, C. The neural basis of functional brain imaging signals. *Trends Neurosci.* **25,** 621–625 (2002).
22. Ogawa, S. *et al.* Intrinsic signal changes accompanying sensory stimulation: functional brain mapping with magnetic resonance imaging. *Proc. Natl Acad. Sci. USA* **89,** 5951–5955 (1992).
23. Glover, G. H. Deconvolution of impulse response in event-related BOLD fMRI. *Neuroimage* **9,** 416–429 (1999).
24. Shtoyerman, E., Arieli, A., Slovin, H., Vanzetta, I. & Grinvald, A. Long-term optical imaging and spectroscopy reveal mechanisms underlying the intrinsic signal and stability of cortical maps in V1 of behaving monkeys. *J. Neurosci.* **20,** 8111–8121 (2000).

Supplementary Information is linked to the online version of the paper at www.nature.com/nature.

Acknowledgements We thank: K. Korinek for designing and fabricating much of the dual-wavelength optical imaging hardware; P. P. Mitra for the suggestion of making continuous recordings and the use of the Chronux analysis software; E. M. C. Hillman for insights into brain haemodynamic mechanisms; C. Ma, G. Cantone, J. Ordinario, E. Glushenkova, W. Zhang, and M. Bucklin for help with recordings; E. Seidemann and R. Siegel for technical help during our initial setup; C. D. Gilbert and members of the Mahoney Center and the Center for Theoretical Neuroscience at Columbia University for comments on the manuscript. The work was supported by the Keck foundation, grants from the National Institutes of Health, the Klingenstein Foundation, the Gatsby Initiative in Brain Circuitry and the Dana Foundation to A.D. and a National Research Service Award to Y.B.S.

Author Contributions The two co-authors collaborated on almost every aspect of this work.

Author Information Reprints and permissions information is available at www.nature.com/reprints. Correspondence and requests for materials should be addressed to A.D. (ad2069@columbia.edu).

METHODS

Tasks: visual fixation. Two monkeys were trained on a variety of visual tasks with a common periodic fixation schedule cued by fixation point colour. The tasks required only passive fixation during 'fixation on' for juice reward (fixation window: 0.5° radius; monitor distance: 133 cm; fix duration: 4 s within trials of duration ranging from 6 to 30 s; trial duration typically held fixed for a given experiment; on some experiments, trial timing switched in blocks between two or three specific values; in other, control experiments, it was randomized by drawing numbers from a homogenous set). Eye fixation and pupil diameter recorded using an infrared eye tracker[25].

Tasks: auditory control. See Supplementary Fig. 10, auditory pitch discrimination task, in a completely dark room (lacking even the fixation point). The trial sequence was as follows: animal pulls lever (start trial) → fixed delay (range 4–10 s in different experiments) → auditory tone onset → delay (typically 4 s) → tone changes pitch, cue to release lever as quickly as possible (200 ms), for juice reward. Once the animals learned this task they performed trials in rapid succession. Thus we could determine task periodicity by setting the initial delay from lever pull to tone on. The monkey typically continued looking in the general direction of the fixation point (even though none was present), allowing us to track pupil dilation with the infrared camera.

Optical imaging: surgery, recording chambers, artificial dura. After the monkeys were trained on visual fixation tasks, craniotomies were performed over the animals' V1, and glass-windowed stainless steel recording chambers were implanted, under surgical anaesthesia, using standard sterile procedures[24,26], so as to image an area of V1 of about 10 mm covering a visual eccentricity of about 1–5°. The exposed dura was resected and replaced with a soft, clear silicone artificial dura. After the animals had recovered from the surgery, cortical activity from their V1 was optically imaged, routinely, while they engaged in relevant behavioural tasks. Recording chambers and artificial dura were fabricated in our laboratory using published methods[27].

Optical imaging: hardware. The camera was a Dalsa 1M30P (binned to 256 pixels × 256 pixels, 15 frames per second). The frame grabber was an Optical PCI Bus Digital (Coreco Imaging). The software was developed in our laboratory based on a system by V. Kalatsky[28]. The illumination was high-intensity light-emitting diodes (Agilent Technologies, Purdy Technologies), with emission wavelengths centred at 530 and 605 nm, filtered through small individual interference filters (Omega Optical). The lens was a 'macroscope' of back-to-back camera lenses[29] focused on the cortical surface. Image acquisition was continuous, simultaneously recording signals from camera, trial timing and behavioural data (trial onset, stimulus onset, identity and duration, etc., eye position, pupil size, timing of fixation breaks, fixation acquisitions, trial outcomes). Data were analysed offline using custom software (MATLAB).

Optical imaging: image processing. All images were first corrected for residual brain movements by aligning each frame to the first frame (shift + rotation[30]), using blood vessels. Signal means (for example, in Fig. 1b) were obtained by averaging signals over the full area, then dividing by the trial-mean of this average to give the percentage signal change as a function of time in a trial. Images of cortical signal (Figs 1a and 4b and Supplementary Movie) were obtained by aligning image sequences to a selected time point (for example, trial onset) and averaging, frame by frame, across the set of all correct trials. This gave 'movies' of cortical activity at the camera frame rate (7.5 frames per second at each wavelength). For images of stimulus-evoked responses (Fig. 1a) (stimulus: 0.25° bar, flashed on for 1 s at the start of each fixation trial), each frame in the movie was then divided, pixel by pixel, by the mean pre-stimulus image (five frames preceding time = 0 ms). The 'Blank' response in Fig. 1b was obtained the same way, at the same time point (3.3 s after stimulus onset), but on a fixation trial with no stimulus. For imaging the trial-related signal (Fig. 4b and Supplementary Movie), each frame in the movie was divided, pixel by pixel, by the trial mean (average of all images over one trial duration), rather than pre-stimulus image, to give the image of fractional signal change relative to the trial mean (Fig. 4b and Supplementary 9). To get time courses of blood-vessel signal relative to the mean (Fig. 4c), the signal was measured along test lines, sampling veins, arteries and 'parenchyma', and the 'parenchyma baseline' regressed away (Supplementary Fig. 9). To get movies of stimulus-evoked activity, similar movies were obtained of cortical activity aligned to stimulus onset, both for trials with stimulus present ('stimulated') and absent ('blank'). Movie frames were divided by the pre-stimulus baseline of three to five frames immediately preceding stimulus onset to get the overall change in cortical activity after stimulus (Supplementary Fig. 1b). We only included trials where the animal maintained fixation correctly.

Visual stimuli for comparing stimulated versus dark-room responses. Gratings were optimized to stimulate the recorded location, typically 100% contrast, 4c/deg, drifting at 4° per second.

Electrophysiology: hardware, electronics and analysis. Extracellular electrode recordings (plastic-coated tungsten: FHC or tungsten in glass; impedances 300–800 kΩ; Plexon amplifier and recording software) were conducted simultaneously with optical imaging (Supplementary Fig. 1). Penetrations were distributed over imaged V1. Recording sites sampled cortical depths starting from most superficial to about 1500 μm below the pial surface at steps of 200–400 μm (Supplementary Table 1). The electrode signal was split into 'spiking' (100 Hz to 8 KHz bandpass) and LFP (0.7–170 Hz). MUA events were defined as each negative-going crossing of a threshold equal to about four times the root mean square of the baseline obtained while the animal looked at a grey screen (Supplementary Fig. 1).

Electrophysiology: data processing. MUA were binned into 16.67-ms bins and aligned to the haemodynamic traces using simultaneously recorded synch events. LFP data were spectrally decomposed using mtspecgramc (Chronux Toolbox for MATLAB; sliding window of 1 s, a step size of 250 ms, frequency range 10–130 Hz) and interpolated into a continuous power spectrum aligned to the haemodynamic traces. Two-dimensional spectrograms (Fig. 2a bottom) show the trial-triggered mean LFP power normalized by the mean pre-trial power in the dark signal (2 Hz frequency resolution). The LFP time course (Supplementary Figs 4 and 6) shows the bandpass-filtered power, integrated over each relevant frequency band ('low-frequency' 10–56 Hz, or 'high-frequency' 66–130 Hz, avoiding 60 Hz).

Electrophysiology: fitting to haemodynamics. For each electrophysiological measure (MUA, low-frequency LFP, high-frequency LFP) the 'best' kernel predicting haemodynamics from concurrent electrophysiology was calculated (Supplementary Fig. 3). Correct trials were extracted from the continuous time series and concatenated into a continuous series. We modelled the haemodynamic response function (HRF) as a gamma kernel: $HRF(t, T, W, A) = A \times (t/T)^{\alpha} \times \exp[(t-T)/-\beta]$, where $\alpha = (T/W)^2 \times 8.0 \times \log(2.0)$, $\beta = W^2/T/8.0/\log(2.0)$, A is the amplitude, T is the time to peak and W is the full width at 75% maximum. We fit the kernel parameters using a downhill simplex algorithm (fminsearch, MATLAB) by comparing the actual haemodynamic response obtained during stimulated trials to that predicted from a convolution of the HRF with the corresponding spike or gamma-band (66–130 Hz) LFP trace. The algorithm reliably converged to similar temporal HRF parameters across all days ($T = 2.50$ (0.08) s, $W = 1.68$ (0.06) s). The proportion of the variance in the haemodynamic responses explained by neuronal activity was quantified using the R^2 statistic from linear regression of the predicted haemodynamic trace to the observed trace both for the stimulated and the dark-room trials.

Controls for trial timing. We performed control experiments to verify that the observed signals were tied specifically to task-related trial onsets, independent of other timing signals. We confirmed that the signal periodicity was not linked to the animal either acquiring or breaking fixation: the two time points, during each trial, with any change in light on the retina (albeit minuscule). This also ruled out any links to extra-retinal fixation-related V1 activity. We controlled for the rhythmic pupil dilations, that is, for the possibility that cortical signals were being evoked by the accompanying pulse of extra light. Giving the animal simulated pupil dilations—a bright flash in the fixation point—evoked no cortical response. As a control for the possibility that the signal was an accidental match to ongoing oscillations, we introduced 20% jitter in trial timing; the signal specifically entrained to trial onsets.

25. Matsuda, K., Nagami, T., Kawano, K. & Yamane, S. A new system for measuring eye position on a personal computer. *Soc. Neurosci. Abstr.* **26**, 744.2 (2000).
26. Das, A. & Gilbert, C. D. Long-range horizontal connections and their role in cortical reorganization revealed by optical recording of cat primary visual cortex. *Nature* **375**, 780–784 (1995).
27. Arieli, A., Grinvald, A. & Slovin, H. Dural substitute for long-term imaging of cortical activity in behaving monkeys and its clinical implications. *J. Neurosci. Methods* **114**, 119–133 (2002).
28. Kalatsky, V. A. & Stryker, M. P. New paradigm for optical imaging: temporally encoded maps of intrinsic signals. *Neuron* **38**, 529–545 (2003).
29. Ratzlaff, E. H. & Grinvald, A. A tandem-lens epifluorescence macroscope: hundred-fold brightness advantage for wide-field imaging. *J. Neurosci. Methods* **36**, 127–137 (1992).
30. Lucas, B. D. & Kanade, T. in *Proc. 7th Int. Joint Conf. Artificial Intelligence* 674–679 (1981).